IMPROVED SOURCE RECONSTRUCTION TECHNIQUE FOR ANTENNA DIAGNOSTICS

E. Jørgensen[1], **P. Meincke**[1], **C. Cappellin**[1], **and M. Sabbadini**[2]

[1]*TICRA, Læderstræde 34, DK-1201 København K, Denmark, ej@ticra.com, pme@ticra.com, cc@ticra.com*
[2]*ESA/ESTEC, 2200 AG Noordwijk, The Netherlands, Marco.Sabbadini@esa.int*

ABSTRACT

This paper presents an improved inverse Method of Moment technique that allows surface currents to be reconstructed on the surface of an antenna. The input to the algorithm is measured near- or far-fields and the method therefore allows antenna engineers to perform antenna diagnostics by inspection of extreme near-fields or antenna currents. The new method provides higher accuracy and is more robust against noise than previously published methods.

Key words: Inverse Method of Moments, antenna diagnostics, source reconstruction, higher-order basis functions.

1. INTRODUCTION

The Inverse Method of Moments (INV-MoM) has attracted considerable attention as a promising technique for performing reconstruction of antenna surface currents based on measured fields. The reconstructed currents can be used for antenna diagnostics, near-field transformations, or for artificial removal of undesired contributions in antenna measurements. The INV-MoM is an inverse-source problem which is a challenging and inherently ill-posed problem to solve. However, the INV-MoM has no hard limit on the resolution of the reconstructed currents whereas traditional microwave holography and mode-based techniques are typically limited to a resolution of $\lambda/2$ when using far-field input data. This makes the INV-MoM the most suitable method for high-accuracy antenna diagnostics on small and medium-sized antenna where the computational cost is manageable.

The INV-MoM has been investigated by several authors [1]-[13] in the past decade. The vast majority of these works have used a discretization scheme based on the well-known RWG basis functions and have formulated an over-determined system of equations that relates the field radiated by each basis function to the field measured at the field sample points. This matrix system is then solved via the truncated singular value decomposition (TSVD) or by means of a conjugate-gradient based iterative solver. However, it was shown recently that these methods reconstruct equivalent currents that are not directly related to the physical fields on the surface of reconstruction. Instead, the reconstructed currents are plagued by an arbitrary choice of fields inside the surface of reconstruction and the methods in [1], [3]-[11] are therefore applicable to far-field to near-field or near-field to near-field transformations, but not to antenna diagnostics problems. This ambiguity is not addressed by most authors and none of the works [1]-[11] have included quantitative comparisons or error estimates of the reconstructed surface currents.

The formulation ambiguity discussed above can be avoided by enforcing the zero-field condition inside the surface of reconstruction which was done for rotationally symmetric problems in [2] and for 3D problems in [12, 13]. These works enforced the zero-field condition by means of a point-matching procedure on a $\lambda/10$ inward surface to the surface of reconstruction. Both [2] and [12, 13] used TSVD to regularize the ill-posed problem and [12, 13] presented quantitative error estimates for the surface currents, achieving a relative RMS error of about 10 percent when using noiseless far-field input data. This paper presents a new approach that differs from existing works in terms of the applied discretization scheme, the enforcement of the boundary condition, and the regularization scheme. The discretization scheme adopted here employs higher-order basis functions and higher-order geometry modeling providing a smooth description of the currents and the geometry, respectively. In addition to a reduction of the required computational resources, the higher-order formulation leads to more stable solutions even in some cases that are not solvable by a piecewise linear current representation provided by the RWG functions. In this work, the boundary condition is enforced *on* the actual surface of reconstruction by means of a quasi-Galerkin testing scheme which requires fewer test functions than the point matching procedure and avoids the need for finding an inward offset surface. Finally, we use the Generalized TSVD method which provides a robust regularization scheme for the inverse problem, in which the a priori knowledge originating from the boundary condition is used independently from the measured data. We also show how the optimal

regularization parameter can be determined automatically during the reconstruction process - an important practical issue which was not adressed in [1]-[13] . The new algorithm is tested using synthetic measured data with added noise and quantitative comparisons with the exact surface currents are presented.

2. FORMULATION OF THE INVERSE PROBLEM

The inverse source problem is aimed at computing tangential electric and magnetic fields on the reconstruction surface S enclosing an antenna, based on fields measured at discrete points outside the surface. On the reconstruction surface, the equivalent electric and magnetic surface current densities are defined as

$$\mathbf{J}_S = \hat{\mathbf{n}} \times \mathbf{H} \tag{1a}$$

$$\mathbf{M}_S = -\hat{\mathbf{n}} \times \mathbf{E}, \tag{1b}$$

where $\mathbf{E}$ and $\mathbf{H}$ are the fields just outside the surface of reconstruction. These equivalent currents are those corresponding to Love's equivalence principle since they produce zero field inside S. They also correspond to the tangential physical fields one would actually measure on S.

The measured field can now be written as

$$\mathbf{E}^{\text{meas}}(\mathbf{r}) = -\eta_0 \mathcal{L}\mathbf{J}_S + \mathcal{K}\mathbf{M}_S \tag{2}$$

where η_0 is the free-space impedance and the integral operators $\mathcal{L}$ and $\mathcal{K}$ are defined as

$$\begin{aligned} \mathcal{L}\mathbf{J}_S = j\omega\mu_0 \Bigg[& \int_S \mathbf{J}_S(\mathbf{r}') G(\mathbf{r},\mathbf{r}')\, dS' \\ & + \frac{1}{k_0^2} \int_S \nabla'_S \cdot \mathbf{J}_S(\mathbf{r}') \nabla G(\mathbf{r},\mathbf{r}')\, dS', \Bigg] \end{aligned} \tag{3a}$$

$$\mathcal{K}\mathbf{M}_S = \int_S \mathbf{M}_S(\mathbf{r}') \times \nabla G(\mathbf{r},\mathbf{r}')\, dS', \tag{3b}$$

where k_0 is the free-space wavenumber and $G(\mathbf{r},\mathbf{r}')$ is the scalar Green's function of free space. Equation (2) is referred to as the data equation, since it relates the measured data $\mathbf{E}^{meas}$ and the unknown surface current densities $\mathbf{J}_S$ and $\mathbf{M}_S$. This inverse problem has been formulated previously by several authors, including [1], [3]-[11].

Love's equivalent currents in (1) constitute just one set of possible equivalent currents that radiate exactly the same field $\mathbf{E}^{\text{meas}}$ outside the reconstruction surface, but different fields $\mathbf{E}_1, \mathbf{H}_1$ inside. The formulation is thus ambiguous and the desired physical current densities in (1), corresponding to Love's equivalence principle, can only be obtained if additional a priori information is imposed. This fact was first noted by Persson *et al.* [2] and a more detailed treatment was presented by Araque Quijano and Vecchi [13]. The desired currents in (1) are obtained by inforcing the a priori information that the fields $\mathbf{E}_1$, $\mathbf{H}_1$ radiated by ($\mathbf{J}_S$,$\mathbf{M}_S$) inside S must be zero [2, 12, 13]. The formulation of the required boundary condition for the electric and magnetic fields leads to the equation

$$-\eta_0 \hat{\mathbf{n}} \times \mathcal{L}\mathbf{J}_S + \left(\hat{\mathbf{n}} \times \mathcal{K} + \frac{1}{2}\right) \mathbf{M}_S = 0, \tag{4a}$$

$$-\left(\hat{\mathbf{n}} \times \mathcal{K} + \frac{1}{2}\right) \mathbf{J}_S - \frac{1}{\eta_0} \hat{\mathbf{n}} \times \mathcal{L}\mathbf{M}_S = 0 \tag{4b}$$

for $\mathbf{r} \in S$. These expressions are referred to as the boundary condition equation.

3. DISCRETIZATION

The surface of reconstruction is discretized using curvilinear patches of up to fourth order. The electric and magnetic surface currents on each patch are expanded as

$$\mathbf{X} = \sum_{m=0}^{M^u} \sum_{n=0}^{M^v-1} a^u_{mn} \mathbf{B}^u_{mn} + \sum_{m=0}^{M^v} \sum_{n=0}^{M^u-1} a^v_{mn} \mathbf{B}^v_{mn} \tag{5}$$

where $\mathbf{X} = [\mathbf{J}, \mathbf{M}]$, a^u_{mn} and a^v_{mn} are unknown coefficients, M^u and M^v are the expansion orders along the u- and v-directions, and $\mathbf{B}^u_{mn}$ and $\mathbf{B}^v_{mn}$ are u- and v-directed vector basis function defined as

$$\mathbf{B}^u_{mn}(u,v) = \frac{\mathbf{a}_u}{\mathcal{J}_s(u,v)} \widetilde{P}_m(u)\, P_n(v)\,, \tag{6a}$$

$$\mathbf{B}^v_{mn}(u,v) = \frac{\mathbf{a}_v}{\mathcal{J}_s(u,v)} \widetilde{P}_m(v)\, P_n(u)\,. \tag{6b}$$

Herein, $\mathbf{a}_u$ and $\mathbf{a}_v$ are the covariant unitary vectors and $\mathcal{J}_s(u,v) = |\mathbf{a}_u \times \mathbf{a}_v|$ is the surface Jacobian. In (6), the polynomials $P_n(v)$ along the direction transverse to the current flow are chosen to be Legendre polynomials due to their nice orthogonality properties. In the direction along the current flow, modified Legendre polynomials [14] are used since they allow the normal current continuity to be enforced. The current expansion above is then inserted in the data equation (2). In order to arrive at a matrix equation, we choose two orthogonal test vectors $(\hat{\theta}, \hat{\phi})$ at each measurement sampling point. This readily leads to the matrix equation

$$\bar{\mathbf{A}}\mathbf{x} = \mathbf{b}, \tag{7}$$

where $\mathbf{x}$ is a vector of unknown basis function coefficients, $\mathbf{b}$ contains samples of the measured field, and $\bar{\mathbf{A}}$ is an $M \times N$ matrix with elements representing the field radiated by a particular basis function.

The current expansion is also inserted in the boundary condition equation (4). In order to arrive at a matrix equation, we choose the testing functions

$$\mathbf{T}^u_{mn}(u,v) = \mathbf{a}^u \widetilde{P}_m(u)\, P_n(v)\,, \tag{8a}$$

$$\mathbf{T}^v_{mn}(u,v) = \mathbf{a}^v \widetilde{P}_m(v)\, P_n(u)\,. \tag{8b}$$

In this expression, $\mathbf{a}^u$ and $\mathbf{a}^v$ are the contravariant unitary vectors. This testing scheme is quasi-Galerkin in the

sense that the basis and testing functions span the same polynomial space on rectangular patches but not in the general case. The contravariant unitary vectors are orthogonal to the covariant unitary vectors and it was found that this choice performed better than pure Galerkin testing. By taking the inner product of the testing functions and (4), we arrive at the matrix equation

$$\bar{\mathbf{L}}\mathbf{x} = \mathbf{0}, \tag{9}$$

where $\bar{\mathbf{L}}$ is a $P \times N$ matrix, whose elements represent the field radiated by a particular basis function, weighted by a particular testing function. The matrix is typically chosen to be square so that $P = N$.

The discretization described above differs from previous published works in two important aspects:

1. The geometry and unknown currents are represented by smooth polynomial functions. This results in improved efficiency, enhanced accuracy, and better resolution properties of the algorithm (see Section 5.3). Previous works are limited to flat patches and piecewise linear basis functions.
2. The testing of the boundary condition operator is performed *on* the actual surface of reconstruction. The previous works that include the boundary condition operator [2, 12, 13] employed an $\lambda/10$ inward offset version of the surface of reconstruction, and Dirac delta functions were used on this surface. This approach introduces ill-conditioning of the matrix $\bar{\mathbf{L}}$, more testing functions are needed, and the inward offset surface is not readily available in practical cases.

4. REGULARIZATION

The data equation (2) is a linear Fredholm integral equation of the first kind (IFK) with compact kernel [15]. It is well-known that its solution is ill-posed in the sense of Hadamard [16],[17, p. 4], so that small perturbations of data due to noise cause arbitrarily large perturbations of the solution.

The matrix equation (7) represents a discrete ill-posed problem and the singular values of $\mathbf{A}$ therefore decay to zero without any gap in the spectrum [17, p. 20]. To obtain a well-posed solution to the problem $\min \|\bar{\mathbf{A}}\mathbf{x}-\mathbf{b}\|_2$ regularization is needed by imposing a priori information about the solution. In this work we suggest to use the a priori information obtained from the fact that the desired currents on the reconstruction surface should satisfy the boundary condition, that is, $\|\bar{\mathbf{L}}\mathbf{x}\|_2$, obtained from the boundary condition equation (4), should be small. Hence, the chosen regularization method not only ensures that the desired Love's equivalent currents are obtained, but also serves the purpose of making the solution well-posed. This differs from previously published works, as will be explained below in Section 4.2.

4.1. Truncated Generalized Singular Value Decomposition

One proper tool for solving the considered regularization problem is the generalized singular value decomposition (GSVD) of the matrix pair $(\bar{\mathbf{A}}, \bar{\mathbf{L}})$. The GSVD constitutes a generalization of the SVD, and takes on the form [18, p. 493]

$$\bar{\mathbf{A}} = \bar{\mathbf{U}} \begin{bmatrix} \bar{\mathbf{\Sigma}} & \mathbf{0} \\ \mathbf{0} & \bar{\mathbf{I}}_{N-P} \end{bmatrix} \bar{\mathbf{X}}^{-1}, \quad \bar{\mathbf{L}} = \bar{\mathbf{V}}(\bar{\mathbf{M}}, \mathbf{0})\bar{\mathbf{X}}^{-1}, \tag{10}$$

in which $\bar{\mathbf{U}}$ has dimension $M \times N$, $\bar{\mathbf{V}}$ has dimension $P \times P$, $\bar{\mathbf{X}} = (\mathbf{x}_1, \ldots, \mathbf{x}_n)$ has dimension $N \times N$, and $\bar{\mathbf{I}}_{N-P}$ denotes the identity matrix of dimension $N - P$. Moreover, $\bar{\mathbf{\Sigma}}$ and $\bar{\mathbf{M}}$ are $P \times P$ diagonal matrices,

$$\bar{\mathbf{\Sigma}} = \text{diag}(\sigma_1, \ldots, \sigma_P), \tag{11}$$

$$\bar{\mathbf{M}} = \text{diag}(\mu_1, \ldots, \mu_P), \tag{12}$$

where $0 < \sigma_1 \leq \cdots \leq \sigma_P \leq 1$, $1 \geq \mu_1 \geq \cdots \geq \mu_P > 0$, and $\sigma_i^2 + \mu_i^2 = 1$. Note that $\bar{\mathbf{U}}$, $\bar{\mathbf{V}}$, and $\bar{\mathbf{\Sigma}}$ are different from the matrices with the same symbols usually used in the SVD of $\bar{\mathbf{A}}$. The existence of the GSVD in the form (10) requires that $\text{rank}\left(\begin{bmatrix} \bar{\mathbf{A}} \\ \bar{\mathbf{L}} \end{bmatrix}\right) = N$ and $\text{rank}\left(\bar{\mathbf{L}}\right) = P$, which is the case for the problem considered here. When $\bar{\mathbf{L}}$ equals the identity matrix, the GSVD is equivalent to the SVD of $\bar{\mathbf{A}}$.

The truncated GSVD (TGSVD) regularized solution $\mathbf{x}_k$ is introduced in [18, p. 494] as a straightforward extension of the truncated SVD (TSVD), in which the components in the solution corresponding to the $P - k$ smallest σ_i are neglected,

$$\mathbf{x}_k = \sum_{i=P-k+1}^{P} \frac{\mathbf{u}_i^H \cdot \mathbf{b}}{\sigma_i} + \sum_{i=P+1}^{N} \mathbf{u}_i^H \cdot \mathbf{x}_i, \tag{13}$$

$k = 1, \ldots, P$. The last term herein, in which $\mathbf{x}_i$ denotes the i'th columns of $\bar{\mathbf{X}}$, belongs to the null space of $\bar{\mathbf{L}}$ and equals zero when $\bar{\mathbf{L}}$ is square, that is, when $P = N$. Expression (13) reveals the ill-posedness of the problem, since small perturbations in $\mathbf{b}$ caused by noise will be amplified by the division of the small values of σ_i. When the regularization parameter k is small, no such small values of σ_i are included, and an over-regularized solution is obtained. On the other hand, when k is large, the solution is under-regularized. The determination of the optimum regularization parameter is discussed in Section 4.3. Another well-suited regularization method for the problem under consideration is that by Tikhonov in general form in which $\bar{\mathbf{A}}$ and $\bar{\mathbf{L}}$ are again treated separately. This general form of the Tikhonov regularization differs from the commonly applied simplified Tikhonov in standard form where $\bar{\mathbf{L}}$ implicitly equals the unit matrix. The application of Tikhonov regularization to the problem at hand is treated in [19].

4.2. Regularization in Standard Form

The regularization problem in which $\bar{\mathbf{L}}$ equals the identity matrix $\bar{\mathbf{I}}_N$ is said to be in standard form [18]. This formulation enforces the a priori information that $\|\bar{\mathbf{x}}\|_2$ should be small (minimum norm solution) and therefore tends to exclude components of $\mathbf{x}$ belonging to the numerical null space $\mathcal{N}(\bar{\mathbf{A}})$ of $\bar{\mathbf{A}}$. The standard form formulation is used in previous works on the considered inverse problem [1], [3]-[11] in which the boundary condition is not enforced. Love's equivalent surface current densities are not obtained from the minimum norm solution since this solution requires components in $\mathcal{N}(\bar{\mathbf{A}})$, as also noted by [12].

In [2, 12, 13] this boundary condition is taken into account by forming a new matrix $\begin{bmatrix}\bar{\mathbf{A}}\\ \bar{\mathbf{L}}\end{bmatrix}$ and applying regularization in standard form on this matrix with the underlying strategy to eliminate the ambiguity of the formulation due to the internal fields $\mathbf{E}_1, \mathbf{H}_1$ by forming the new matrix and subsequently making the solution stable by the regularization. The approach taken in this paper is different in that we keep the data matrix $\bar{\mathbf{A}}$ and the boundary condition matrix $\bar{\mathbf{L}}$ separate and use the latter to combat both the formulation ambiguity and the instability. Section 5.2 below compares the performance of these two approaches.

4.3. Choosing the Optimum Regularization Parameter

Much work has been reported in the literature on determining the optimum regularization parameter for discrete ill-posed problems. One of the most reliable approaches is the L-curve method [20]. The key idea in this method is to realize that the solution norm $\eta = \|\bar{\mathbf{L}}\mathbf{x}_k\|_2$, plotted versus the residual norm $\delta = \|\bar{\mathbf{A}}\mathbf{x_k} - \mathbf{b}\|_\mathbf{2}$ as function of k in a logarithmic scale, is a monotonically increasing function and forms the shape of an L. An example of such an L-curve is shown in Fig. 1. When k is small, the solution is over-regularized, and (η, δ) is on the lower-right part of the L-curve. Similarly, when k is large, (η, δ) is on the upper-left part. The optimum value of k is that corresponding to the L-curve corner.

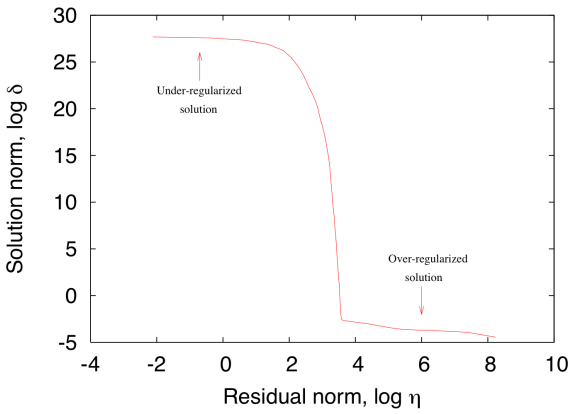

Figure 1. Example of L-curve. The optimum regularization parameter is the value of k corresponding to the corner.

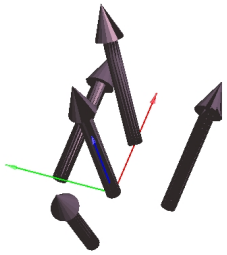

Figure 2. The considered array consisting of five Hertzian dipole elements. The x-axis is in red, the y-axis in green, and the z-axis in blue. Information about the elements are given in Tab. 1.

Position (x, y, z) [λ]	Orientation (θ, ϕ) [deg]	Excitation [A]	Type
$(0, 0, 0)$	(20,40)	$1\angle 0°$	Electric
$(-0.1, 0, 0)$	(-10,0)	$1\angle 30°$	Magnetic
$(0.1, 0, 0)$	(45,30)	$1\angle 0°$	Electric
$(0, 0.1, 0)$	(90,0)	$1\angle 0°$	Electric
$(0, -0.1, 0)$	(90,0)	$1\angle 0°$	Magnetic

Table 1. Position, orientation, excitation, and type of the five dipoles in Fig. 2.

5. NUMERICAL RESULTS

To validate our algorithm two canonical cases are considered. These cases are described in this section and Sections 5.1 - 5.3 then illustrate various properties of the algorithm.

Case 1 involves an array of five electric/magnetic Hertzian dipoles with a pseudo-random volumetric distribution as shown in Fig. 2. The far field radiated by the array is calculated and used as input to the INV-MoM method. The electric and magnetic surface current densities, $\hat{\mathbf{n}} \times \mathbf{H}$ and $-\hat{\mathbf{n}} \times \mathbf{E}$, respectively, are reconstructed on a sphere with centre at the origin and radius 0.3λ.

Case 2 involves an array of three y-polarised Huygen's sources located in the xy-plane as shown in Fig. 3. The separation distance d is here chosen to be $\lambda/4$. The three sources are enclosed in a box of height $\lambda/5$ and the field is observed on the top face of the box, which is at $z = 0.1\lambda$.

For both cases the relative root mean square (RMS) error,

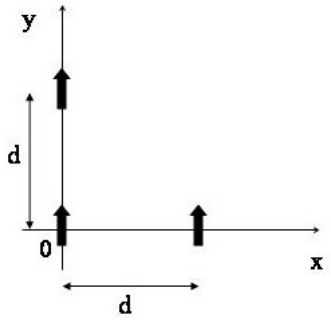

Figure 3. Three Huygen's sources separated by the distance $d = \lambda/4$.

RMS_E, between reconstructed and exact electric fields, $\mathbf{E}_{\text{rec}}$ and $\mathbf{E}_{\text{exact}}$, is determined by

$$\text{RMS}_E = \sqrt{\frac{\int_S |\hat{\mathbf{n}} \times \mathbf{E}_{\text{rec}} - \hat{\mathbf{n}} \times \mathbf{E}_{\text{exact}}|^2 \, dS}{\int_S |\hat{\mathbf{n}} \times \mathbf{E}_{\text{exact}}|^2 \, dS}}, \qquad (14)$$

and RMS_H is calculated similarly. Uncorrelated Gaussian noise, specified by the signal to noise ratio SNR, is added to the real and imaginary parts of the calculated far fields before performing the reconstruction.

5.1. Convergence of RMS Error

The higher-order discretization implies that the unknown surface current densities can be more accurately described by increasing the polynomial order of the discretization. Consequently, the relative RMS error should decrease as the polynomial order increases. To illustrate that this is indeed the case, RMS_E and RMS_H are calculated for Case 1 with no noise as function of the polynomial order using the TGSVD solution $\mathbf{x}_k$ from (13). The results are shown in Tab. 2. From these results it is seen that the RMS error decreases by approximately a factor of 10 when the polynomial order is increased from 1 to 2 and another factor of 10 when increasing the order from 2 to 3. The error also decreases when going from 3 to 4, but for polynomial order 5 the RMS error is higher than that for polynomial order 3. The convergence of the RMS error breaks down because the discretized problem becomes so ill-posed that an accurate solution no longer can be obtained. The lowest relative RMS error obtained by this method is about 0.3 percent.

5.2. Impact of Noise

Tab. 3 shows the relative RMS errors RMS_E and RMS_H for Case 1 for various SNRs when solving the standard form problem from [2, 12, 13] using TSVD, as described in Section 4.2, and also the general form problem in (13) using TGSVD regularization. Polynomial order 3 is used for the discretization. In both cases the L-curve method is applied to determine the optimum regularization parameter. It is seen that the error increases with decreasing SNR for both methods, as expected. It is also observed that the regularization method suggested in this work is very robust against noise and that it performs better than the previously suggested method employed in [2, 12, 13] for any polynomial order. When the TGSVD is used, the problem remains solvable even for severe noise levels.

5.3. Resolution of INV-MoM

We now investigate whether distinct sources separated by a small electrical distance can be accurately resolved by the INV-MoM. Case 2 is suitable for this purpose and the box-shaped surface of reconstruction is discretized using 16 patches. The number of unknowns and the required number of far field sampling points are listed in Tab. 4. The electric field on the $z = 0.1\lambda$ plane exhibits a rapid variation and even the best-possible approximation with the given set of basis functions may not be an accurate representation of the exact fields. To illustrate this, we show both the exact field and the best possible approximation with the current set of basis functions. The latter solution has been obtained by forward MoM. All plots in this section shows the y-component of the electric field.

	$d = \lambda/4$
Reconstruction surface (box)	$\lambda/2 \times \lambda/2 \times \lambda/5$
Patches	16
Polynomial order	5
Unknowns	1440
Far-field sampling points	720

Table 4. Parameters for the two cases with three Huygen's sources separated by a distance d.

The results for a separation of $\lambda/4$ are presented in Fig. 4. The exact field is shown in Fig. 4a whereas Fig. 4b shows a projection of the exact field onto the fifth-order basis functions. Therefore, Fig. 4b shows ideal reconstructed field for the present discretization. It can be seen by comparing Figs. 4a and Fig. 4b that the 5th-order polynomial expansion has problems along the horizontal center line. This problem can be recognized in the reconstructed field for noise-less far field data which is shown in Fig. 4c. The reconstructed field is in good agreement with the best possible field for the present discretization in Fig. 4b, although the three sources appear slightly closer together. The reconstructed field for noisy far field data (SNR=60 dB) is shown in Fig. 4d. The two lower sources can no longer be distinguished whereas the third source is clearly identifiable.

The case reported here, as well as other cases reported in [19], indicate that there is no hard limit on the resolution. In the noise-less condition, the field can be reconstructed nearly without loss of information and sources

	1	2	3	4	5
RMS$_E$, TGSVD	0.18	0.02	0.006	0.002	0.04
RMS$_H$, TGSVD	0.28	0.03	0.008	0.003	0.06

Table 2. RMS$_E$ and RMS$_H$ as function of polynomial order for Case 1.

	Noiseless	50 dB	40 dB	30 dB	20 dB
RMS$_E$, std. form	0.02	0.07	0.20	0.62	1.94
RMS$_E$, gen. form	0.006	0.07	0.08	0.19	0.20
RMS$_H$, std. form	0.03	0.07	0.20	0.64	2.02
RMS$_H$, gen. form	0.008	0.06	0.07	0.17	0.19

Table 3. Relative RMS errors for various SNRs when using the standard-form regularization method from [2, 12, 13] (std. form) and the general-form method of this paper (gen. form).

can be clearly separated, although small artifacts may occur. For noisy data, sources separated by $\lambda/4$ may or may not be identifiable. It is interesting to note that traditional microwave holography typically operates with a minimum pixel size of $\lambda/2$. The entire field of view in Fig. 4 would correspond to a single pixel when using microwave holography.

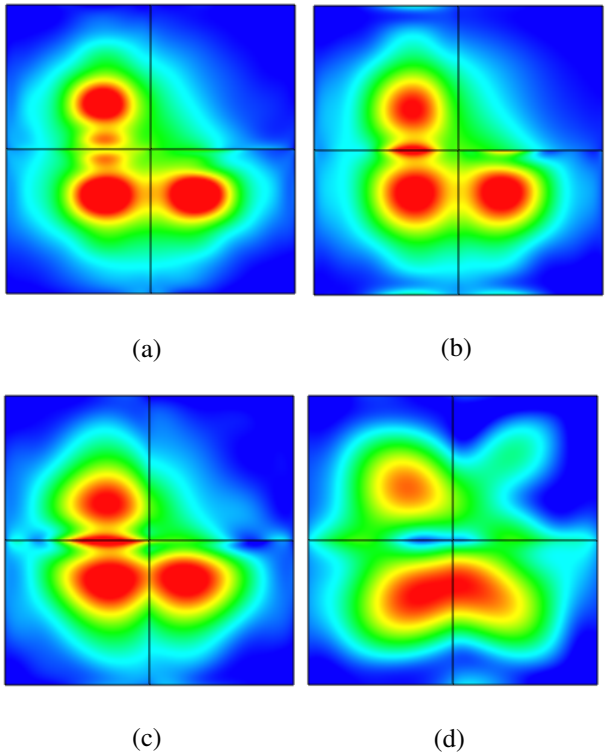

Figure 4. Electric field from three Huygen's sources separated by a distance of $\lambda/4$. (a) The reference field. (b) The best possible field for the present discretization. (c) Field reconstructed from far field data without noise. (d) Field reconstructed from far field data with SNR=60 dB.

6. CONCLUSIONS

This paper has presented an improved INV-MoM that uses curved patches and higher-order basis functions, quasi-Galerkin testing of the boundary condition equation, as well as a robust regularization scheme based on the TGSVD and an automated method for determining the optimum regularization parameter. The performance of the algorithm has been tested on a few canonical cases and the relative RMS error obtained is 1-2 orders of magnitude lower than previously published works. In addition, it was shown that the method can reconstruct the field from discrete sources with a separation smaller than $\lambda/2$, even when starting from far-field data with practical noise levels. Further investigations, including comparisons with low-order methods and other regularization schemes, will be published in [19].

ACKNOWLEDGMENTS

This work is supported by ESTEC within the ARTES 3/4 programme, ESTEC contract 22676/09/NL, DIATOOL - Development of an antenna diagnostics tool.

REFERENCES

1. Sarkar, T.K. & Taaghol, A. (1999). Near-field to near/far-field transformation for arbitrary near-field geometry utilizing and equivalent electric current and MoM, *IEEE Trans. Antennas Propagat.*, **47(3)**, pp. 566–573.

2. Persson, K. & Gustafsson, M. (2005). Reconstruction of equivalent currents using a near-field data transformation - with radome applications, *Progress in Electromagnetics Research*, **54**, pp. 179–198.

3. Las-Heras, F. & Sarkar, T.K. (2006). Evaluating near-field radiation patterns of commercial antennas, *IEEE Trans. Antennas Propagat.*, **54(8)**, pp. 2198–2207.

4. Alvarez, Y., Las-Heras, F. & Pino, M.R. (2007). Reconstruction of equivalent currents distribution over arbitrary three-dimensional surfaces based on integral equation algorithms, *IEEE Trans. Antennas Propagat.*, **55(12)**, pp. 3460–3468.

5. Alvarez, Y., T, K, S. & Las-Heras, F. (2007). Improvement of the sources reconstruction techniques: Analysis of the svd algorithm and the rwg basis functions, in *IEEE Antennas and Propagation Society International Symposium*, Honolulu, Hawaii, USA.

6. Alvarez, Y., Las-Heras, F., Pino, M.R. & Lopez, J.A. (2008). Acceleration of the sources reconstruction method via the fast multipole technique, in *IEEE Antennas and Propagation Society International Symposium*, San Diego, CA, USA.

7. Mioc, F., Quijano, J.A., Vecchi, G., Martini, E., Milani, F., Guidi, R., Foged, L.J. & Sabbadini, M. (2008). Source modelling and pattern enhancement for antenna farm analysis, in *30th ESA Antenna Workshop on Antennas for Earth Observation, Science, Telecommunication and Navigation Space Missions*, Noordwijk, The Netherlands, 555–559.

8. Eibert, T.F. & Schmidt, C.H. (2009). Multilevel fast multipole accelerated inverse equivalent current method employing rao-wilton-glisson discretization of electric and magnetic surface currents, *IEEE Trans. on Antennas Propag.*, **57(4)**, pp. 1178–1185.

9. Lopez, Y.A., Andres, F.L.H., Pino, M.R. & Sarkar, T.K. (2009). An improved super-resolution source reconstruction method, *IEEE Trans. Instrumentation and Measurement*, **58(11)**, pp. 3855–3866.

10. Schmidt, C.H., Ismatullah & Eibert, T.F. (2010). Comparison of lower and higher order basis functions in inverse equivalent current methods, *Applied Computational Electromagnetics Society (ACES) Conference, Tampere, Finland*.

11. Alvarez, Y., Las-Heras, F. & Pino, M.R. (2010). Antenna characterization using the sources reconstruction method, in *EuCAP Proceedings*, Barcelona, Spain.

12. Quijano, J.L.A. & Vecchi, G. (2009). Improved-accuracy source reconstruction on arbitrary 3-D surfaces, *IEEE Antennas and Wireless Propagation Letters*, **8**, pp. 1046–1049.

13. Quijano, J.L.A. & Vecchi, G. (2010). Field and source equivalence in source reconstruction on 3D surfaces, *Progress in Electromagnetics Research*, **PIER-103**, pp. 67–100.

14. Jørgensen, E. (2003). *Higher-Order Integral Equation Methods in Computational Electromagnetics*, ph.d. thesis, ISBN 87-91184-21-5, Technical University of Denmark, Ørsted-DTU, Lyngby, Denmark.

15. Wing, G.M. (1991). *A primer on integral equations of the first kind*, Society for Industrial and Applied Mathematics, Philadelphia, PA.

16. Hadamard, J. (1923). *Lectures on Cauchy's Problems in Linear Partial Differential Equations*, Yale University Press, New Haven, CT.

17. Hansen, P.C. (1998). *Rank-Deficient and Discrete Ill-Posed Problems*, Society for Industrial and Applied Mathematics, Philadelphia, PA.

18. Hansen, P.C. (1989). Regularization, GSVD and truncated GSVD, *BIT*, **29**, pp. 491–504.

19. Jørgensen, E. & Meincke, P. (2010). Higher-order inverse MoM with robust regularization for accurate antenna diagnostics, *submitted to IEEE Transactions on Antennas and Propagation*.

20. Hansen, P.C. (1992). Analysis of discrete ill-posed problems by means of the L-curve, *SIAM Review*, **34**, pp. 561–580.